SYNOPSIS OF THE THESIS

ABSTRACT

The thesis describes a facile synthesis of silver nanoparticles (AgNPs) within both aqueous and non-aqueous microemulsions with very high optical quality, which are subsequently used to perform several photophysical studies. The content of the thesis has been spread into seven chapters. In *Chapter 1,* a brief introduction of optical properties of metal nanoparticles (MNPs), structural and dynamical characteristics of microemulsions, primarily formed by an anionic surfactant sodium dioctylsulfosuccinate (AOT) and its applications in synthesis of various nanoparticles is provided. Details of instrumental techniques and measurement methods have been summarized in *Chapter 2*. In *Chapter 3*, a facile synthesis protocol is demonstrated to obtain superior optical quality AgNPs inside water/AOT/*n*-heptane reverse micelles (RMs). The growth of the AgNP within the RMs core may severely influence the structural organization of the reverse micellar interface. The modification of the interfacial layer associated with nanoparticle formation has been probed by a solvatochromic probe coumarin 343 (C343) in the *Chapter 4.* In the *Chapter 5,* application of superior optical quality AgNPs is demonstrated in plasmon- fluorophore interaction by exploiting the natural confinement of RM to act simultaneously as a template for AgNP and to host the fluorophores. In the succeeding *Chapters,* I intend to produce high optical quality AgNPs inside a non-aqueous acetonitrile/AOT/*n*-heptane microemulsion. However, nature of the microemulsion template remains debated in the literature and hence, first probed the morphology of the acetonitrile microemulsion at different w_s (= [acetonitrile]/[AOT]) using a solvatochromic probe 4-aminophthalimide (4-AP) in *Chapter* 6. It is observed that the microemulsion undergoes a morphological transition from RM to bicontinuous microemulsion (BMC) above a certain w_s. Finally, in *Chapter* 7, synthesis of AgNPs has been performed in the microemulsion at various w_s and it is found that structural and optical properties of the synthesized AgNPs correlate nicely with the microemulsion template morphology proposed in the *Chapter 6.*

CHAPTER 1: INTRODUCTION

The fascinating optical properties of MNPs arise from surface plasmon resonance (SPR), which are a collective oscillation of free electrons clouds.[1-4] In this chapter, I provided a brief overview of MNPs SPR, theoretical and experimental techniques for SPR measurements, uniqueness of AgNPs SPR compared to all other MNPs and its implications in plasmonic applications. SPR of MNPs has the ability to interact with closely spaced molecular fluorophore and this phenomenon is known as plasmon-fluorophore (PF) interaction.[5-6] The concept and necessary conditions for PF interaction and its implications on various photophysical processes of a fluorophore are discussed. In this chapter, I also reviewed several interesting reports of PF interaction involving various metal nanostructures with an emphasis on the confined systems (MNPs in micelles, block copolymers and RMs).

The nano-confined core of microemulsion acts as a nanoreactor for material synthesis and provide numerous advantage (exceptional control over size, aniosotropy and shape) compared to other synthetic methods.[7-12] Here I provide a brief overview of various types of microemulsion (polar and non-polar) and different phases of microemulsion with RM as sub-phase.[13-15] Numerous surfactants are used in RMs formation however; sodium dioctylsulfosuccinate (AOT) is most popular as RMs are formed without aid of co-surfactant.[13, 16] The structure and properties of AOT RMs and transition of RMs to bi-continuous microemulsion (BMC) are briefly discussed. Here I provide a brief overview of general synthetic procedure, necessary conditions and mechanism of nanoparticles formation inside AOT RM.[9-10, 17] In this chapter, I also reviewed several interesting reports on the optical properties AgNPs synthesized by AOT reverse micellar route. Nanoparticle formation inside AOT RMs induce significant changes in their structural organizations and I presented several interesting reports on this.[7, 18-19]

CHAPTER 2: MATERIALS, METHODS AND INSTRUMENTATION

In this chapter, I mentioned sources of all chemicals that are used in our studies. Various sample preparation procedures, data analysis methods are given. Here I also provided specifications of all the instruments used in our works including UV-Vis

spectroscopy, steady-state and time-resolved fluorescence spectroscopy, transmission electron microscopy (TEM) and dynamic light scattering (DLS) etc.

CHAPTER 3: A FACILE SYNTHESIS OF HIGH OPTICAL QUALITY SILVER NANOPARTICLES BY ASCORBIC ACID REDUCTION INSIDE AOT REVERSE MICELLES

In this *Chapter*, our effort on developing an exceptionally easy method to fabricate high optical quality AgNPs is presented by using ascorbic acid (AA) as a reducing agent inside AOT RM at w_0 values of 2, 6 and 10. For the first time, it is shown that RM can support a chemical reduction that cannot proceed in aqueous medium at room temperature. Simply, addition of $AgNO_3$ and AA solutions into AOT/*n*-heptane mixtures leads to formation of AgNPs at room temperature in the absence of inert atmosphere or prolonged stirring. The optical quality of the SPR band of AgNPs are found to be superior compared to AgNPs obtained by common reducing agents like sodium borohydride or hydrazine under similar conditions. TEM and DLS measurements shows that the nanoparticles are spherical, and are slightly larger than the pure RMs. In addition, the size and the polydispersity gradually increase with increase in the w_0 value.

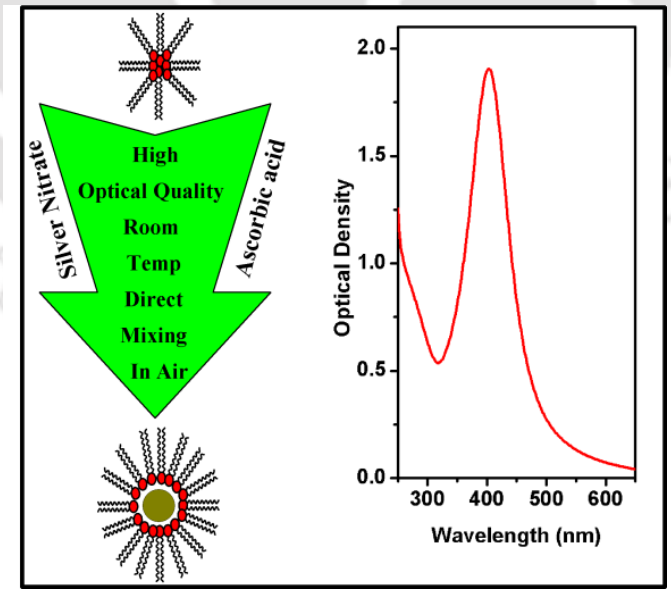

Figure 3.1: Schematic representation of superior optical quality silver nanoparticles synthesized inside water/AOT/n-heptane reverse micellar systems.

CHAPTER 4: SELECTIVE PROBING OF THE INTERFACIAL REGION OF AOT REVERSE MICELLE UPON NANOPARTICLE FORMATION USING DYNAMIC STOKES SHIFT MEASUREMENTS

In the previous *Chapter*, it is demonstrated that superior optical quality AgNPs can be easily synthesized inside AOT reverse micellar assemblies. However, the grown AgNPs may severely influence the structural organization of the original RMs interface. In this *Chapter*, I probed the hydration and organization of the interfacial layer using a site-selective hydrophilic probe, coumarin 343 (C343). I have characterize of the interfacial layer of water/AOT/*n*-heptane RMs before and after AgNPs formation by combination of steady-state absorption, excitation, emission spectroscopy, time-resolved fluorescence anisotropy and dynamic stokes shift measurements. It is observed that both solvation dynamics and rotational dynamics inside the interfacial region of the RM become significantly faster upon AgNPs formation, particularly at low w_0 (at w_0=2) but at higher w_0 values dynamics of the AgNPs containing RM becomes nearly identical to the pure RM. The results indicate that the interfacial region of the RMs becomes more hydrated, less packed upon nanoparticle formation particularly at low w_0 value. The results are in accordance with the significant size change of the RM to accommodate the nanoparticle at low water content.

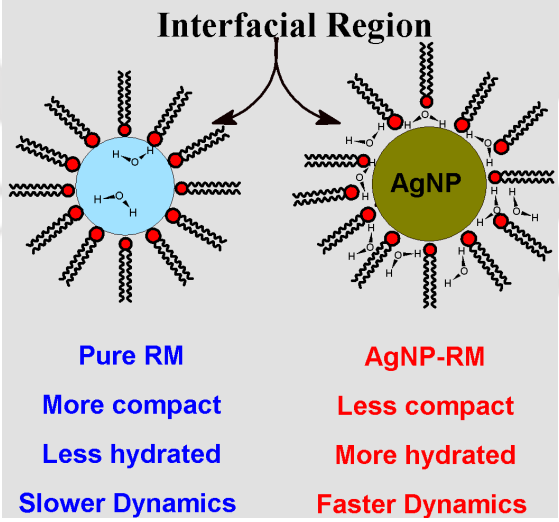

Figure 4.1: A schematic representation of perturbation of reverse micellar interface before and after formation of silver nanoparticles inside the reverse micelles.

CHAPTER 5: INTERACTION OF MOLECULAR TRANSITION WITH SURFACE PLASMON RESONANCE OF SILVER NANOPARTICLE INSIDE RESTRICTED ENVIRONMENT OF AOT REVERSE MICELLE

In this *Chapter*, the utility of high optical quality AgNPs in plasmon- fluorophore interaction is demonstrated by exploiting the natural confinement of a RM to act simultaneously as a template for AgNPs formation and to host the fluorophores. The fluorophores, fluorescein (FL) and safranine O (SAF) and reducing agent (AA) are loaded together into the water pool; thereafter, silver salt was added and subsequently, spectral modification and size evolution are observed by steady-state and time-resolved spectroscopy. In the FL-AgNP composite system, the SPR band of AgNPs undergoes a strong redshift. Moreover, significant modification of both the fluorescence intensity and lifetime of FL is found when AgNPs were gradually formed inside the RM core. On the contrary, in the SAF-AgNP composite, no such effect is noticed and the composite system retains the original optical characteristics of their constituents. This differential effect has been rationalized by dissimilar plasmon-fluorophore coupling in the two systems controlled by a combination of different spatial distribution and spectral detuning of the molecular absorption maxima of the dyes (455 nm and 530 nm for FL and SAF, respectively) from the SPR band maximum (~400 nm) of AgNPs.

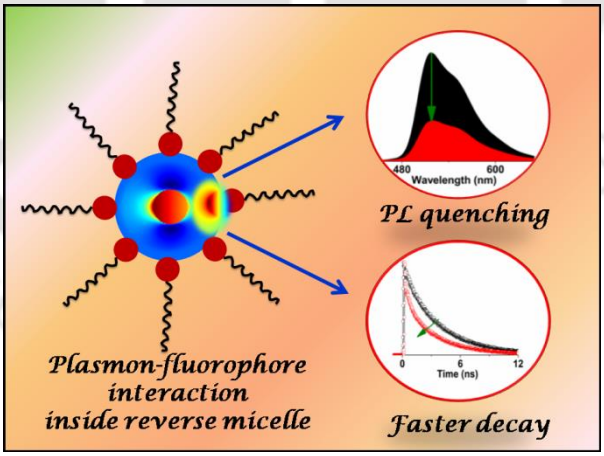

Figure 5.1: A schematic representation plasmon- fluorophore interaction and its implications on the emission properties of fluorescein inside restricted environment of AOT reverse micelles.

CHAPTER 6: ANOMALOUS SPECTRAL BEHAVIOR OF 4-AMINOPHTHALIMIDE INSIDE NON-AQUEOUS ACETONITRILE MICROEMULSION: IMPLICATION ON REVERSE MICELLE TO BI-CONTINUOUS MICROEMULSION TRANSITION

Now I try to explore new methods to produce high optical quality AgNPs in non-aqueous environment. As $AgNO_3$ exhibits very high solubility in acetonitrile, acetonitrile/AOT/*n*-heptane microemulsion is chosen as a template for synthesis of AgNPs. However, microemulsion morphology of the template remains debated in the literature and hence in this *Chapter*, I first investigated the debated acetonitrile/AOT/*n*-heptane microemulsion whether it exists as RMs or BMC, using a hydrophilic solvatochromic fluorophore 4-aminophthalimide (4-AP) at different w_s (= [acetonitrile]/[AOT]). Herein, it is observed that the emission properties vary anomalously at lower and higher w_s regions. The quantum yield (ϕ_f) and lifetime (τ_f) of 4-AP first increase up to w_s = ~1, and thereafter, decrease upon further increase in the w_s values. The emission maximum of 4-AP shifts to higher wavelength from 445 nm at w_s = 0 to 475 nm at w_s = 8. Interestingly, unlike aqueous RMs, the emission maximum at w_s = 1 matches with the emission maximum in neat acetonitrile and the emission maximum shifts to even longer wavelength at higher w_s. Steady-state anisotropy also shows a break around w_s = 1; anisotropy decreases very sharply from w_s = 0 to 1, and

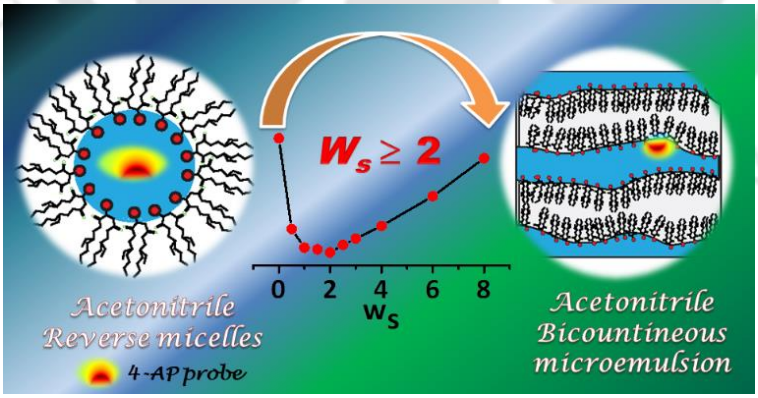

Figure 6.1: Systematic representation of reverse micelles to bi-continuous microemulsion transition of the acetonitrile/AOT/*n*-heptane microemulsion with gradual increment in the acetonitrile content (w_s).

afterward remains constant. Solvation dynamics becomes gradually faster with increase of the acetonitrile content only in the low w_s regimes but remains almost independent of w_s after $w_s > 2$. All of the results clearly indicate that the morphology of the microemulsion may change at an intermediate w_s (~1); below this, the system behaves like RMs and above this, the system may remain as BMC.

CHAPTER 7: HYDROPOBIC SILVER NANOPARTICLE SYNTHESIS INSIDE ACETONITRILE MICROEMULSION AND ITS IMPLICATION IN PROBING THE STRUCTURAL TRANSITION OF THE MICROEMULSION

In the previous *Chapter*, it is observed that acetonitrile/AOT/*n*-heptane microemulsion may undergo structural transition from RM to BMC after certain w_s. Herein, a unique strategy is developed for probing of this transition by using microemulsion itself as a template for synthesis of silver colloids. Precursors (silver nitrate) and reducing agents (AA) are insoluble in *n*-heptane phase and thus, Ag colloids formation occur solely inside the acetonitrile fraction and therefore, the structural morphology of the Ag colloids provides valuable information regarding the structure of the template where Ag colloids formation occur. The synthesized AgNPs were found to be very stable at dry conditions and exhibit very high optical quality compared to all other AOT microemulsion based synthesis methods (both aqueous and non-aqueous).

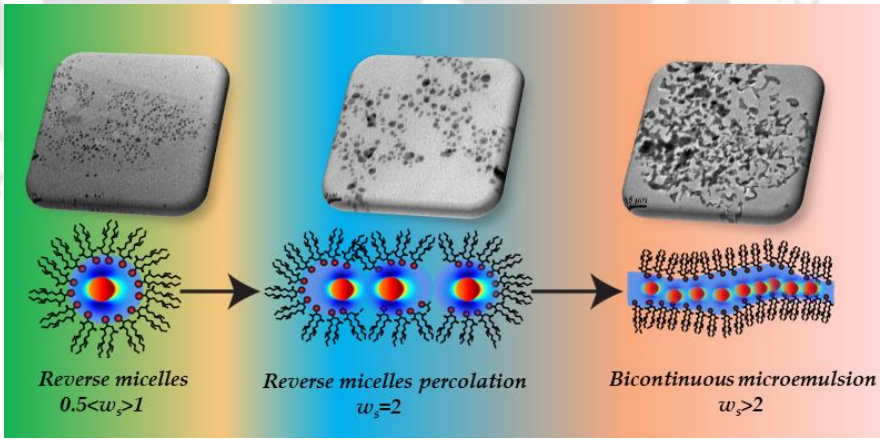

Figure 7.1: Systematic representation of evidence of transformation of reverse micellar structure to the bi-continuous microemulsion of acetonitrile/AOT/n-heptane microemulsion through *in situ* silver nanoparticles synthesized inside systems at different w_s.

At low w_s (≤ 1), synthesized silver colloids exhibits remarkably strong SPR band but the strength of SPR remarkably drops at $w_s = 2$ and almost vanishes at $w_s = 3$. TEM measurements revealed the presence of isolated spherical monodispersed AgNPs of ~6 nm diameter at lower w_s and larger distribution of nanoparticle sizes at $w_s = 2$. Most interestingly, interconnected Ag colloids packed channels were found at $w_s = 3$ which directly shows footprint of the BMC nature of the microemulsion template. Thus, the characteristics of Ag colloids (i.e. size distribution and optical quality) provide valuable information about interfacial structure of the microemulsion and suggested that microemulsion switches from RM to BMC nature at an intermediate w_s.

SUMMARY AND FUTURE OUTLOOK

In the present thesis a facile synthesis method has been developed to obtain high optical quality AgNPs inside aqueous and non-aqueous (acetonitrile) AOT microemulsion. This has been achieved by using a mild reducing agent ascorbic acid (AA). To the best of our knowledge, the optical quality of the AgNPs synthesized by this route was found to be much superior than previously reported other aqueous and non-aqueous AOT microemulsion routes. The synthesized AgNPs were found to be highly stable, redispersable and even retained optical quality in coated form. The high optical quality of AgNPs is effectively used in selective probing the interfacial region of microemulsion, plasmon-fluorophore interaction and probing acetonitrile microemulsion structure. This work is expected to open new avenue towards synthesis of various other metal nanoparticles, bimetallic nanoparticles, metal oxides and sulphide nanoparticles etc. It will be very interesting to see the optical properties of other metal nanoparticles especially copper and gold synthesized by this route. A detailed summary and future outlook is provided in the end of the thesis.

REFERENCES

1. Mulvaney, P., Surface Plasmon Spectroscopy of Nanosized Metal Particles. *Langmuir* **1996**, *12*, 788-800.
2. Kelly, K. L.; Coronado, E.; Zhao, L. L.; Schatz, G. C., The Optical Properties of Metal Nanoparticles: The Influence of Size, Shape, and Dielectric Environment. *J. Phys. Chem. B* **2003**, *107*, 668-677.
3. Henry, A.-I.; Bingham, J. M.; Ringe, E.; Marks, L. D.; Schatz, G. C.; Van Duyne, R. P., Correlated Structure and Optical Property Studies of Plasmonic Nanoparticles. *J. Phys. Chem. C* **2011**, *115*, 9291-9305.
4. Mayer, K. M.; Hafner, J. H., Localized Surface Plasmon Resonance Sensors. *Chem. Rev.* **2011**, *111*, 3828-3857.
5. Lakowicz, J. R., *Principles of Fluorescence Spectroscopy*; Springer: New York, 2006.
6. Lakowicz, J. R.; Ray, K.; Chowdhury, M.; Szmacinski, H.; Fu, Y.; Zhang, J.; Nowaczyk, K., Plasmon-Controlled Fluorescence: A New Paradigm in Fluorescence Spectroscopy. *Analyst* **2008**, *133*, 1308-1346.
7. Setua, P.; Ghatak, C.; Rao, V. G.; Das, S. K.; Sarkar, N., Dynamics of Solvation and Rotational Relaxation of Coumarin 480 in Pure Aqueous-Aot Reverse Micelle and Reverse Micelle Containing Different-Sized Silver Nanoparticles inside Its Core: A Comparative Study. *J. Phys. Chem. B* **2012**, *116*, 3704-3712.
8. Wang, C.-y.; Liu, C.-y.; Wang, Y.; Shen, T., Spectral Characteristics and Photosensitization Effect on Tio2of Fluorescein in Aot Reversed Micelles. *J. Colloid. Int. Sci.* **1998**, *197*, 126-132.
9. Zhang, W.; Qiao, X.; Chen, J., Synthesis and Characterization of Silver Nanoparticles in Aot Microemulsion System. *Chem. Phys.* **2006**, *330*, 495-500.
10. Zhang, W.; Qiao, X.; Chen, J.; Wang, H., Preparation of Silver Nanoparticles in Water-in-Oil Aot Reverse Micelles. *J. Colloid. Int. Sci.* **2006**, *302*, 370-373.
11. Solanki, J. N.; Murthy, Z. V. P., Controlled Size Silver Nanoparticles Synthesis with Water-in-Oil Microemulsion Method: A Topical Review. *Industrial and Engineering Chemistry Research* **2011**, *50*, 12311-12323.
12. Petit, C.; Lixon, P.; Pileni, M. P., In Situ Synthesis of Silver Nanocluster in Aot Reverse Micelles. *J. Phys. Chem.* **1993**, *97*, 12974-12983.
13. Correa, N. M.; Silber, J. J.; Riter, R. E.; Levinger, N. E., Nonaqueous Polar Solvents in Reverse Micelle Systems. *Chem. Rev.* **2012**, *112*, 4569-4602.
14. Elles, C. G.; Levinger, N. E., Reverse Micelles Solubilizing Dmso and Dmso/Water Mixtures. *Chem. Phys. Lett.* **2000**, *317*, 624-630.
15. Riter, R. E.; Undiks, E. P.; Kimmel, J. R.; Levinger, N. E., Formamide in Reverse Micelles: Restricted Environment Effects on Molecular Motion. *J. Phys. Chem. B* **1998**, *102*, 7931-7938.
16. Brown, D.; Clarke, J. H. R., Molecular Dynamics Simulation of a Model Reverse Micelle. *J. Phys. Chem.* **1988**, *92*, 2881-2888.
17. Bagwe, R. P.; Khilar, K. C., Effects of Intermicellar Exchange Rate on the Formation of Silver Nanoparticles in Reverse Microemulsions of Aot. *Langmuir* **2000**, *16*, 905-910.

LIST OF PUBLICATIONS

Paper included in this thesis:

1. **Singha, D.;** Barman, N.; Sahu, K., A Facile Synthesis of High Optical Quality Silver Nanoparticles by Ascorbic Acid Reduction in Reverse Micelles at Room Temperature. *J. Colloid. Int. Sci.* **2014**, *413*, 37-42.
2. **Singha, D.;** Barman, N.; Phukon, A.; Sahu, K., Selective Probing of Reverse Micelle Interfacial Layer Upon Silver Nanoparticle Formation Using Dynamic Stokes Shift Measurements. *J. Phys. Chem. C* **2014**, *118*, 10366-10374.
3. **Singha, D.;** Sahu, D. K.; Sahu, K., Coupling of Molecular Transition with the Surface Plasmon Resonance of Silver Nanoparticles inside the Restricted Environment of Reverse Micelles. *ACS Omega* **2017**, *2*, 5494-5503.
4. **Singha, D.;** Sahu, D. K.; Sahu, K., Anomalous Spectral Modulation of 4-Aminophthalimide inside Acetonitrile/AOT/n-Heptane Microemulsion: New Insights on Reverse Micelle to Bicontinuous Microemulsion Transition. *J. Phys. Chem. B* **2018**, *122*, 6966-6974.
5. **Singha, D.;** Sahu, D. K.; Sahu, K., Probing the Interfacial Transition of Acetonitrile/AOT/*n*-heptane Microemulsion Through *in situ* Silver Colloid Synthesis**.** *Colloids Surf. A* ***2019****, 574, 171-177.*

Paper not included in this thesis:

1. Barman, N.; **Singha, D.**; Sahu, K., Fluorescence Quenching of Hydrogen-Bonded Coumarin 102-Phenol Complex: Effect of Excited-State Hydrogen Bonding Strength. *J. Phys. Chem. A* **2013**, *117*, 3945-3953**.**
2. Barman, N.; **Singha, D**.; Sahu, K., Faster Photoinduced Electron Transfer in a Diluted Mixture Than in a Neat Donor Solvent: Effect of Excited-State H-Bonding. *Phys. Chem. Chem. Phys.* **2014**, *16*, 6159-6166.
3. Sahu, D. K.; **Singha, D**.; Sahu, K., Sensing of Iron(Iii)-Biomolecules by Surfactant-Free Fluorescent Copper Nanoclusters. *Sens Biosensing Res.* **2019**, *22*, 100250.

LIST OF CONFERENCE PROCEEDINGS

1. International Conference on Advanced Nanomaterial and Nanotechnology (**ICCAN 2013).**
   Organized by center of Nanotechnology, Indian institute of technology, Guwahati.
2. Recent Trends in Fundamental and Applied Chemical Sciences ***(RTFACS-14)***
   Organized by Dibrugarh University
3. International Symposium Advances in Spectroscopy and Ultrafast Dynamics ***(ASUD 2014)***.
   Organized by Indian Association of Cultivation of Science, Kolkata.
4. Frontiers in Chemical Sciences ***(FICS 2014)***
   Organized by department of chemistry, Indian institute of technology, Guwahati.
5. **Reflux 2015.**
   Organized by department of chemical engineering, Indian institute of technology, Guwahati.
6. **Reflux 2018.**
   Organized by department of chemical engineering, Indian institute of technology, Guwahati.

LIST OF SCHEMES

Scheme 6.1: Representation of RM and bi-continuous microemulsion models along with the chemical structures of the surfactant sodium 1,4-bis(2-ethylhexyl)sulfosuccinate (AOT) and the fluorophore 4-aminophthalimide (4-AP).

Scheme 6.2: Systematic conversation of acetonitrile/AOT/*n*-heptane reverse microemulsion to bi-continuous microemulsion with gradual addition acetonitrile.

Scheme 7.1: Template-directed expected growth of silver nanoparticles within acetonitrile/AOT/*n*-heptane microemulsion at different w_s.

LIST OF FIGURES

implication in PF interaction. (b) Probe location dependent interaction between 2-AS (fluorophore) and AuNPs in micelles of triblock copolymers of F127 and P123.

Figure 1.9: Schematic representation modification of microemulsion structures from w/o droplets to o/w droplets with increase in the amount of water content (w_0). Note that there is an intermediate phase where oil and water together known as bi-continuous phase.

Figure 1.10: Comparison of optical quality of the AgNPs SPR band at w_0=10 by the work of (a) Petit et al. with (b) Bagwe et al work. Petit et al. used $NaBH_4$ reduction in NaAOT by using(– – –) silver nitrate and (–) silver sulfosuccinate as silver precursor, $[AOT]_{total}$=0.1 M; $[AgNO_3]$= [AgAOT]=10^{-3} M, $[NaBH_4]$= 10^{-4} M. Bagwe et al used $NaBH_4$ reduction in NaAOT by using silver nitrate as a precurssor, $[AgNO_3]$= 1.8×10^{-3} M, $[NaBH_4]$= 9×10^{-4} M in presence of different surfactant additives.

Figure 1.11: Spectra showing (a) a relation between of SPR bandwidth with particle diameters synthesized by AOT microemuslion route using $NaBH_4$ and N_2H_4 (hollow circle) as reducing agents. The dash line represents Mie simulation curve. (b) Variation of SPR peak with w_0 values of AOT microemulsion. Note that a blue shift in SPR maxima is noticed with increase in w_0 values.

Figure 1.12: Schematic representation of probing of AOT reverse micellar interface before and after AgNPs formation inside (a) non-aqueous ethylene glycol and (b) aqueous reverse micelles**.**

Figure 3.1: The UV-Vis spectra of water/AOT/n-heptane reverse micellar systems at w_0 = 2,6 and 10 containing different additives- (a) water, (b) 0.3 mM $AgNO_3$, (c) 0.3 mM $AgNO_3$ and 0.01 mM AA, (d) 0.3 mM $AgNO_3$ and 0.05 mM AA, (e) 0.3 mM $AgNO_3$ and 0.10 mM AA, and (f) 0.3 mM $AgNO_3$ and 0.20 mM AA. All concentrations represent the overall concentration. The inset represents snapshots of these solutions when viewed under ordinary light.

Figure 3.2: Comparison of the UV-Vis spectra of the AgNP formed in the water/AOT/n-heptane reverse micellar systems at different w_0 values (a) w_0 = 2, (b) w_0 = 6, and w_0 = 10. The overall concentrations of AOT, $AgNO_3$ and AA were 90, 0.30

and 0.10 mM, respectively. The inset represents snapshots of these solutions when viewed under ordinary light.

Figure 3.3: Comparison of optical quality of SPR band of AgNP at w_0 =10 obtained in this work with Petit et al (a) Present work by AA reduction using [AOT]=0.09 M, $[AgNO_3]=0.3\times10^{-3}$ M, $[AA]=0.5\times10^{-4}$ M (b) By Petit et al. via $NaBH_4$ reduction in NaAOT by using(– – –) silver nitrate and (–) silver sulfosuccinate as silver precursor. $[AOT]_{total}$=0.1 M; $[AgNO_3]$= [AgAOT]=10^{-3} M, $[NaBH_4]= 10^{-4}$ M

Figure 3.4: UV-Vis spectra of the AgNPs formed in the water/AOT/n-heptane reverse micellar systems at w_0 = 6 showing the effect of different reducing agents (top) $NaBH_4$ and (bottom) $N_2H_4.H_2O$ at different concentrations of the reducing agents; 0.05, 0.1, 0.3 mM. The overall concentrations of AOT and $AgNO_3$ were 90 and 0.30 mM, respectively. The inset represents snapshots of these solutions when viewed under ordinary light.

Figure 3.5: Size distributions obtained from dynamic light scattering (DLS) measurements at different w_0 values for pure reverse micelles, and reverse micelles containing the synthesized AgNPs.

Figure 3.6: TEM images and size distribution histograms of AgNPs synthesized by AA reduction at (a) w_0 = 2, (b) w_0 = 6 and (c) w_0 = 10, respectively. The overall concentrations of $AgNO_3$ and AA were 0.30 and 0.10 mM, respectively.

Figure 4.1: The UV-visible spectra of water/AOT/n-heptane reverse micellar system at w_0 = 6 comprising (a) AgNPs only (black), (b) C343 and AgNPs (red), (c) C343 only (blue). The green curve represents the difference spectrum [(b)-(c)]. The absorption spectrum of C343 in the pure reverse micelle and the difference spectrum are compared in a magnified scale in the inset.

Figure 4.2: Emission spectra of coumarin 343 (C343) at various excitation wavelengths (λ_{ex}) for the pure and the AgNP containing RMs at w_0= 2. The plot of the emission maxima against λ_{ex} for the two cases are shown in the inset.

Figure 4.3: Absorption spectrum (black), excitation spectra using a standard 10 mm cuvette (red) and in a glass capillary tube (0.8 mm internal diameter) (green) of C343

in pure RMs (top panel) and in AgNP containing RMs at $w_0 = 2$ (bottom panel). The excitation spectra are recorded at an emission wavelength of 490 nm.

Figure 4.4: TEM images and size distribution histograms of the AgNPs in RMs at w_0=6 in (a) the absence of C343 (top) (b) in the presence of 10 µM C343 (bottom).

Figure 4.5: Fluorescence anisotropy decays, r(t) of C343 recorded at 470 nm and excited at 405 nm in the pure RMs (RM, black) and in the silver nanoparticle containing RMs (AgNP-RM, blue) at different w_0 values.

Figure 4.6: Decay of the solvent response function, C(t) of C343 in pure (o) and silver nanoparticle containing (o) RMs at w_0 values of 2, 6 and 10. The points represent the actual values while the solid lines denote the best fit to bi-exponential decay.

Figure 4.7: Time resolved emission spectra (TRES) and time resolved area-normalised emission spectra (TRANES) spectra of the C343 at different time in pure (RM) and silver nanoparticle containing (AgNP-RM) reverse micellar system at $w_0 = 6$.

Figure 5.1: Evolution of extinction spectra of different systems with time: (a) AgNP inside AOT reverses micelle, (b) AgNP and safranin O in RM (c) AgNP and fluorescein in RM. The variation of SPR maxima with time for various systems is added in plot (d).

Figure 5.2: Normalized UV-visible extinction spectra of only AgNP, only fluorophore and AgNP-fluorophore composite and calculated combined (AgNP+fluorophore) extinction spectrum. Safranine O (SAF) and fluorecein (FL) are respectively used in the top and bottom panels. Extinction spectrum of the AgNP-SAF system has strong similarity with the comibed spectrum but the extinction spectrum of the AgNP-FL system deviates much from the calculated spectrum.

Figure 5.3: Dynamic light scattering measurements of FL-AgNPs composites at different time.

Figure 5.4: Variation of steady state excitation (left panel) and emission intensity of safranin (λ_{ex}= 510, λ_{em}= 570 nm) and fluorescein (λ_{ex}= 445 nm, λ_{em}= 530 nm) in the presence of growing silver nanoparticle with time inside reverse micellar solution. Inset of right panel shows normalized intensity of respective fluorophore and arrow indicates

increase in shoulder peak with time. For clear visibility of peak position in excitation spectrum only spectra before and after complete growth of AgNPs are provided.

Figure 5.5: Fluorescence anisotropy decays, r(t), of safranin (λ_{ex}= 510 nm, λ_{em}= 565 nm) and fluorescein (λ_{ex}= 405 nm, λ_{em}= 520 nm) before and after complete growth of AgNPs.

Figure 5.6: Fluorescence decays of safranin (λ_{ex}= 510 nm, λ_{em}= 565 nm) and fluorescein (λ_{ex}= 405nm, λ_{em}= 520 nm) inside AOT reverse micellar solution, before and after AgNPs nanoparticle formation.

Figure 6.1: (a) Absorption spectra of 4-AP in acetonitrile/AOT/*n*-heptane microemulsion at different w_s. Absorption spectrum of neat acetonitrile (dotted line) is also included for comparison (b) Emission spectra ($\lambda_{ex.}$=360 nm) of 4-AP in acetonitrile/AOT/*n*-heptane microemulsion at different w_s values. Inset shows emission maxima (in nm) vs w_s plot.

Figure 6.2: Variation of the red-edge excitation shift (REES, $\Delta\nu$ in nm) of 4-AP inside acetonitrile/AOT/*n*-heptane microemulsion with gradual increment in the w_s. Inset shows emission spectra of 4-AP at various excitation wavelengths (λ_{ex}) at w_s = 1

Figure 6.3: Steady state fluorescence anisotropy (left panel) of 4-AP inside acetonitrile/AOT/*n*-heptane microemulsion at various acetonitrile contents measured at the emission maxima (λ_{ex}=360 nm). Fluorescence decays of 4-AP (right panel) inside acetonitrile/AOT/*n*-heptane microemulsion at various w_s measured at the corresponding emission maximum (λ_{ex} = 375 nm).

Figure 6.4: The relative shift in time resolved emission maxima $\Delta\,\lambda_{em}^{max} = \lambda_{em}^{max}\,(t = 60\,ns) - \lambda_{em}^{max}\,(t = 0.1\,ns)$ of probe 4-AP in acetonitrile/AOT/*n*-heptane microemulsion at different w_s.

Figure 6.5: (a) Emission spectra and (b) emission maxima (λ_{max}) of 4-AP($\lambda_{ex.}$=360 nm) in acetonitrile solvent as a function of AOT concentration.

Figure 6.6: Hydrodynamic diameter of acetonitrile/AOT/*n*-heptane microemulsion at different w_s values obtained from dynamic light scattering (DLS) measurements. At

low w_s (0-1), mostly single size distribution exists (a) but at high w_s, distribution becomes highly polydispersed (b).

Figure 7.1: The UV-Vis spectra of Ag colloids formed in the acetonitrile/AOT/*n*-heptane microemulsions at w_s = 0.5, 1, 2 and 3. The concentration of $AgNO_3$ and AA is fixed at 0.3 mM and 0.20 mM, respectively. Photographs of each solution are given in the inset.

Figure 7.2: Hydrodynamic diameter of acetonitrile/AOT/*n*-heptane microemulsion at different w_s values obtained from DLS measurements in absence of silver nanoparticles (a) and in presence of AgNP (b). The concentration of $AgNO_3$ and AA is fixed at 0.3 mM and 0.20 mM, respectively.

Figure 7.3: TEM images and size distribution histograms of Ag colloids synthesized by AA reduction at w_s = 0.5, 1, 2 and 3 respectively. The overall concentrations of $AgNO_3$ and AA are 0.30 and 0.20 mM, respectively. Histograms are generated by excluding larger AgNP aggregates and TEM micrograph at w_s =3 are represented in lower resolution (500 nm scale bar).

Figure 7.4: Comparison of UV-Vis spectra of as prepared AgNPs formed in the acetonitrile/AOT/*n*-heptane microemulsions at w_s=0.5 and after evaporation followed by re-dispersing in n-heptane. Photographs of as prepared, evaporated and re-dispersed solutions are given in the inset.

भारतीय प्रौद्योगिकी संस्थान गुवाहाटी
Indian Institute of Technology Guwahati